© Universiti Tun Hussein Onn Malaysia Publisher's Office

IJIE

Jhttp://penerbit.uthm.edu.my/ojs/index.php/ijie
ISSN : 2229-838X e-ISSN : 2600-7916

The International Journal of Integrated Engineering

Numerical Simulation of Temperature Field in Ultra-Narrow Arc Welding of Thick-Walled Steam Turbine Valve Body Material

Gou Ningnian[1], Wang Yaowei[1], Sun Shuo[1],Han Xiaotong[2], Saffirna M.S.[3], Jiang Xiaoxia[1*], Feng Zhourong[4]

[1]School of Mechanical Engineering,
Ningxia University, 750021 Yinchuan, CHINA

[2]Faculty of Mechanical Engineering,
Universiti Teknologi Malaysia, 81310 Johor Bahru Johor, MALAYSIA

[3]Faculty of Mechanical & Automative Engineering Technology,
University Malaysia Pahang, 26600 Pekan, Pahang, MALAYSIA

[4]COCEL Cast Steel Co., LTD, 550 Beijing West Road, Yinchuan, CHINA

DOI: https://doi.org/10.30880/ijie.2022.14.08.016
Received 30 May 2022; Accepted 28 November 2022; Available online 21 December 2022

Abstract: The welding problems of large and thick plates are becoming more prominent as the application of large-scale and thick-plate metal structures grows. Due to the issue of excessive welding deformation between the 60mm thick steam turbine valve body and the pipe joint, a new process method is employed to connect. In this paper, the welding technology of flux strip confined arc ultra-narrow gap is proposed to carry out welding test on the ZG13Cr9Mo2Co1NiVNbNB cast steel test block of steam turbine valve body material with a thickness of 60 mm. The welding temperature field is measured by means of a K-type thermocouple and numerical simulation. The results show that the thermal cycle curve obtained by the homogeneous body heat source simulation is basically consistent with the thermal cycle curve measured during the experiment, and the simulation results of the molten pool morphology are also consistent with the actual macroscopic morphology of the weld.

Keywords: Thick-walled parts, ultra-narrow gap welding, temperature field, numerical simulation

1. Introduction

Numerous large-scale and thick-plate metal structures are being employed more and more frequently as a result of the quick development of contemporary industrial equipment, engineering structures, and other metal structures with high capacities and high parameters [1]. Manual arc welding and carbon dioxide gas shielded welding are currently used in enterprises for the butt joint of large steel castings. The V-shaped groove is opened during welding. There are several consumables. The workload is high, and flaws such as slag inclusion, porosity, undercut, and fractures are common. It needs to be repaired, which is time-consuming and labor-intensive. Especially in the process of thick plate welding, traditional welding methods (manual arc welding, submerged arc welding, etc.) can no longer get high-quality welds due to the limitation of heat input. When a large amount of heat is applied to a weld, the residual stress increases and the grains close the weld grow larger. The welded joint will accelerate the formation of fatigue cracks, brittle fractures, or stress corrosion cracks under the action of tensile load and tensile residual stress [2,3].

*Corresponding author: jiangxx@nxu.edu.cn

The technology of ultra-narrow gap welding with flux strips constraining arc [4] with its lower heat input can effectively inhibit the growth of grains in the heat-affected zone, which leads to a strong, tough, and excellent weld. This welding method is suitable for welding heat-sensitive materials. The ultra-narrow gap welding method of arc ultra-narrow-gap welding through the flux sheet has successfully realized the butt joint of X60 pipeline steel and rail.

At present, the welding method has not been industrialized. A lot of research is still in the experimental stage. To achieve reliable welding parameters, expertise or a series of tests were relied on. However, relying solely on experimental approaches to collect data will take a significant amount of time and money. To limit the number of trials, numerical simulation is employed to calculate the welding temperature field prior to the formulation of the relevant welding process, which serves as a reference for the formulation of an acceptable welding process. Before the appropriate welding process is developed, the welding temperature field is calculated using numerical simulation to minimize the number of experiments. This will provide a reference for formulating a reasonable welding process. Therefore, the numerical simulation of ultra-narrow gap welding with flux strips constraining the arc has important significance.

2. Welding Experiment

2.1 Experimental Materials

The experimental material is the ZG13Cr9Mo2Co1NiVNbNB cast steel test block of the steam turbine valve body material with a 1# test block at 60mm×50mm×150mm and 2# test block at 59mm×63mm×150mm. Table 1 shows the chemical composition of the material. A 3mm thick protrusion is added to the bottom of the 2# test block. The welding groove assembly method is shown in Fig. 1. The welding material is Ø1.6mm CB2 welding wire, and the chemical composition is shown in Table 2.

Table 1 - Chemical composition of ZG13Cr9Mo2Co1NiVNbNB (%)

C	Si	Mn	S	P	Cr	Mo	Co	Ni	V	Nb	N	B
0.13	0.08	0.4	0.002	0.005	9.26	1.5	1.13	0.14	0.20	0.05	0.02	0.009

Table 2 - Chemical composition of CB2 (%)

C	Si	Mn	P	S	Cr	Ni	Co	Mo	V	Nb	B	N
0.13	0.30	0.75	0.015	0.01	9.11	0.20	1.15	1.59	0.21	0.054	0.01	0.015

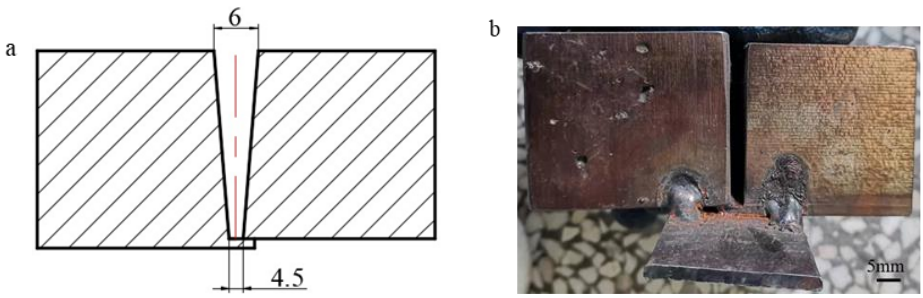

Fig. 1 - (a) Groove diagram; (b) physical map of weldment

2.2 Welding Equipment

The NB-500T inverter gas shielded welding machine is used in the experiment. The test block is fixed during welding, and the welding torch is welded along a fixed track. By designing different auxiliary support and guiding structures, the welding torch can be adapted to different working conditions. Fig. 2 shows the present welding equipment.

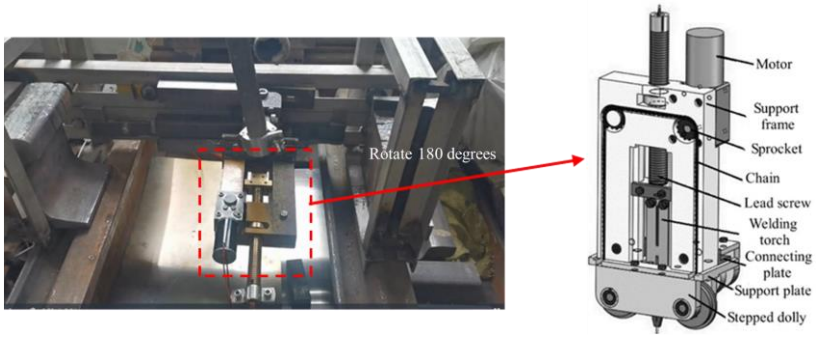

Fig. 2 - Ultra-narrow gap welding device

2.3 Temperature Field Measuring Equipment

As shown in Fig. 3 (a) and (b), the K-type thermocouple wire can measure temperatures of up to 1300 °C, and the temperature field during welding can be measured using a 12V power supply (see Fig. 3c). Because the voltage value generated by the thermocouple wire is very small, the current is about 52mv at 1300 °C, and the signal needs to be amplified by the thermocouple amplifier. Then, using an oscilloscope, read the voltage change curve near the welding torch temperature measurement point. Fig. 3b shows the AD8495 ARMZ amplifier module, which can convert the small voltage generated by the thermocouple node into an easy-to-read signal. The gain at the output of the thermocouple amplifier is 5mV/°C, and the AD8495 uses a temperature sensor to perform cold junction compensation.

Fig. 3 - (a) K-type thermocouple wire; (b) thermocouple amplifier; (c) 12v power supply

As shown in Fig. 4, first use a 12V power supply to power the thermocouple amplifier separately. After fixing the thermocouple wire at the measuring point, connect the positive pole (red wire) of the thermocouple wire with the UCC end of the amplifier. The negative pole (blue wire) should then be connected to GND. The signal is amplified by the thermocouple amplifier; the output terminal's positive and negative poles (OUT, GND) are connected to the oscilloscope's positive and negative poles of the alligator clip; and the amplified electrical signal is finally displayed on the oscilloscope.

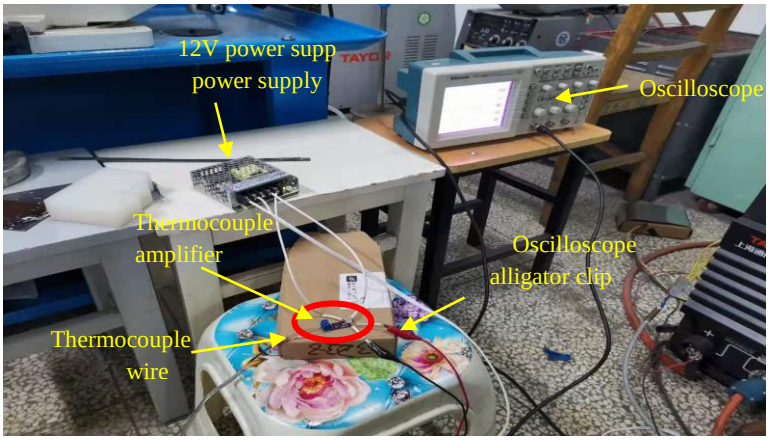

Fig. 4 - Measuring temperature curve equipment

2.4 Welding Parameters

The ultra-narrow gap welding groove is I type. Firstly, the two test blocks are assembled into an I-shape, and the anti-deformation angle is preset during assembly. It is then welded with a 3mm thick backing plate to form an I-shaped groove with an anti-deformation angle, which is controlled at 1.6°~1.8°. Fix the test block to the transverse welding device, then bend and place the flux tape in the U-shaped groove. The reaction force formed by the elasticity of the glass fiber mesh is utilized to make the flux sheet close to the inner wall of the weld groove. After the preparation is completed, an ultra-narrow gap welding experiment will be carried out. To effectively control weld formation and microstructure properties, the weldment is preheated to 250 °C before welding, and the interlayer temperature is kept at around 200 °C. The welding parameters are shown in Table 3.

Table 3 - Welding experiment parameters

Weld bead	Welding voltage (V)	Welding current (A)	Welding speed (mm/s)
(1-5)	22	190	9.0
(6-10)	22	185-190	9.0
(11-15)	22	195	9.0

3. Establish a Finite Element Model of the Welding Temperature Field

3.1 Select The Heat Source Model

The welding heat source must be effectively described and the correct heat source model must be established in order to calculate the welding process using the finite element method. The heat source model is a mathematical representation of the heat source's characteristics and mathematical distribution on the welding bead. It remains to be seen whether the heat source model accurately expresses the determination of the accuracy of the finite element calculation results of the temperature field in the welding process. The uniform body heat source model [5,6] is frequently used to simulate the temperature field of multi-pass welding because it implies that welding heat is consistently distributed in a given heating volume. The heat generation rate at any point in the heat source area is

$$q = \frac{\eta UI}{V} \qquad (1)$$

In the formula, V is the volume of the heat source, m3. When the uniform body heat source model's heat source acting volume V was determined, 1/10 to 1/5 of the entire weld volume was selected for trial calculation [7]. It is necessary to continuously adjust the size of the heat source action volume V to finally obtain a suitable welding temperature field result. The heat source action volume V is the product of the weld bead height, a, the heat source action volume width, b, and the molten pool size, c, as shown in Fig. 5.

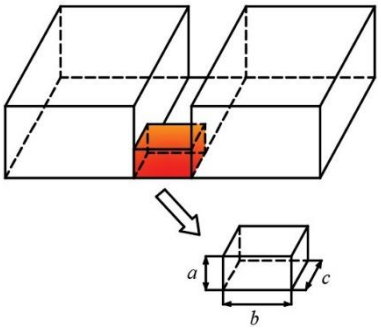

Fig. 5 - Heat source volume

After trial calculation, finally, the heat source action volume is 1/5 of the weld volume, the height a of the heat source action volume is 3mm (filling height), the length c (the length of the molten pool) is 15mm, and the parameter b is 9mm. According to the characteristics of ultra-narrow gap welding with flux strips constraining arc, combined with references, η is taken as 0.9. Incorporate formula (1) to calculate q and get the corrected heat source under different welding parameters (see Table 4).

Table 4 - Welding heat source parameters

Weld bead	Welding voltage (V)	Welding current (A)	Welding heat source (J/m^3)
(1-5)	22	185	9.1×10^9
(6-10)	22	190	9.3×10^9
(11-15)	22	195	9.5×10^9

3.2 Thermophysical Performance Parameters of Materials

The value of these thermophysical properties with temperature must be provided because the simulation of the welding temperature field is a non-linear transient thermal analysis. However, there are few thermophysical performance

parameters at high temperatures. Therefore, the relevant thermophysical parameters of cast steel materials at high temperatures are calculated with the help of JMatPro software. The specific heat, thermal conductivity, and density of the material change with temperature between 20 °C and 1600 °C, as shown in Fig. 6.

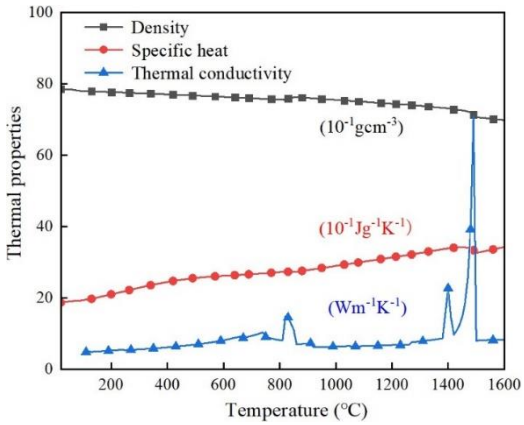

Fig. 6 - Temperature field materials' thermal physical performance parameters

3.3 Establishment of Finite Element Model and Meshing

The size of the built geometric model is 150mm×105mm×63mm, and SOLID70 is used as the thermal analysis element. When dividing the grid, different element division schemes are made for different positions of the test block (weld seam, heat-affected zone, base metal) [8]. The mesh is shown in Fig. 7. The model contains 124083 elements, the number of nodes is 129234, and the weld area has the smallest element size of 1mm×1mm×3mm.

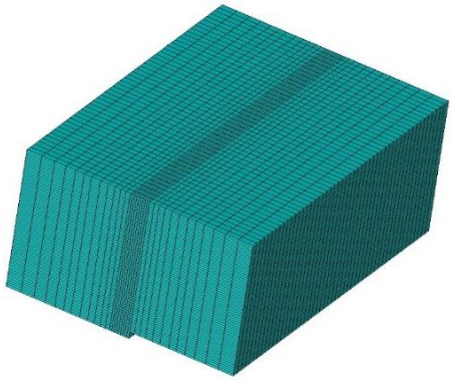

Fig. 7 - The meshing model of the specimen

3.4 Boundary Conditions

Welding heat loss is primarily due to radiation, with convection playing a minor role. Because the radiative heat transfer effect is greatest at higher temperatures, radiation appears mostly around the weld. The radiation equation is highly nonlinear and is different from the convection equation. The total heat transfer coefficient can be used to deal with convection and radiation boundary conditions. The convection and emissivity coefficients are combined and applied to the surface as a composite heat dissipation coefficient [9]. The convection and radiation coefficients are assigned together to form a composite heat dissipation coefficient, and the formula is

$$a_{\mathrm{h}}=\begin{cases}0.0668T, & 0<T<500^{\circ}\mathrm{C}\\ 0.231T-82.1, & T\geqslant 500^{\circ}\mathrm{C}\end{cases} \tag{2}$$

The composite heat dissipation coefficient is denoted by a_{h} in the formula. T is the temperature in degrees Celsius. The composite heat dissipation coefficient that changes with the temperature used in this paper is shown in Table 5.

Table 5 - Composite heat dissipation coefficient

Temperature	20	100	200	300	400	500	700	900	1000	1200	1400	1500
Compound heat dissipation coefficient ($W \cdot m^{-2} \cdot ℃^{-1}$)	1.3	6.68	13.36	20	26.7	33.4	79.6	125.8	148.9	195.1	241.3	264.4

4. Results and Discussion

4.1 Experimental Verification of Calculation Results

The measuring point is located 9mm from the bottom surface of the current weld bead. The results of the numerical simulation and the experimental findings are compared using the thermal cycle curve. In the temperature rising part, the simulation result is found to be similar to the temperature cycle curve measured by the experiment, as shown in Fig. 8. Due to the welding equipment and the anti-deformation setting of the groove, the thermocouple wire cannot directly contact the welding material. Hence, the temperature change rate of the measured thermal cycle curve is smaller than that of the simulated thermal cycle curve.

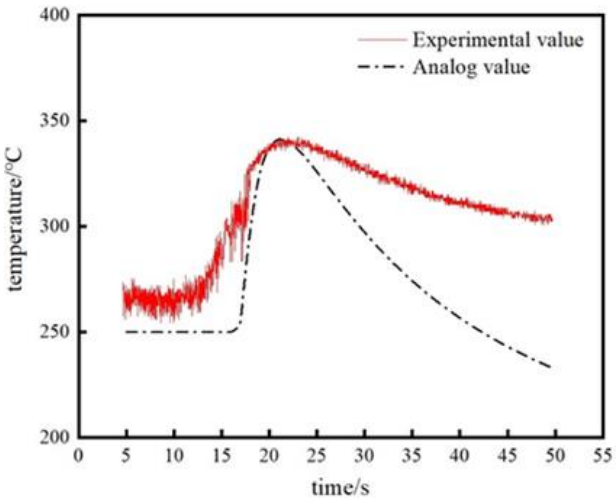

Fig. 8 - Comparison of temperature curves between measured values and simulated values

After welding, the test piece is cut, and the weld cross-section obtained is polished and etched. Fig. 9(a) shows the appearance of the first weld and Fig. 9(b) shows the macroscopic appearance of the weld. The simulation results are analyzed, and the area with a temperature greater than 1400℃ is taken as the molten pool, while the area with a temperature between 800℃ and 1400℃ is designated as the heat-affected zone of the weld. It is then compared to the weld's macroscopic appearance. The shape of the molten pool obtained by numerical simulation, as shown in Fig. 9, is consistent with the cross-sectional shape of the molten pool obtained under experimental conditions. Furthermore, the welding numerical simulation fusion line is identical to the experimental welding fusion line. The molten pool morphology in the simulation results corresponds to the macro morphology of the actual weld.

4.2 Analysis of Welding Temperature Field

The welding temperature field was simulated using finite element simulation on the ZG13Cr9Mo2Co1NiVNbNB cast-steel test block. The temperature field distribution of the weld surface is shown in Fig. 10 at various stages of the welding simulation process. The shape of the temperature field changes as the welding heat source travels, as shown in Fig. 10. The welding heat source has a high temperature, and the welding temperature rises rapidly as the heat source functions to form a molten pool. The temperature of the weldment gradually decreases as the heat source leaves. The high-temperature area continues to move as the heat source moves, resulting in a visible 'tailing' phenomena. As with welding, the range of the temperature field steadily widens, as illustrated in Fig. 10 (b), (c), and (d). As the temperature increases, the faster the heat diffusion, hence, the temperature spreads in the shape of an elliptical arc from the center of the heat source to the surroundings.

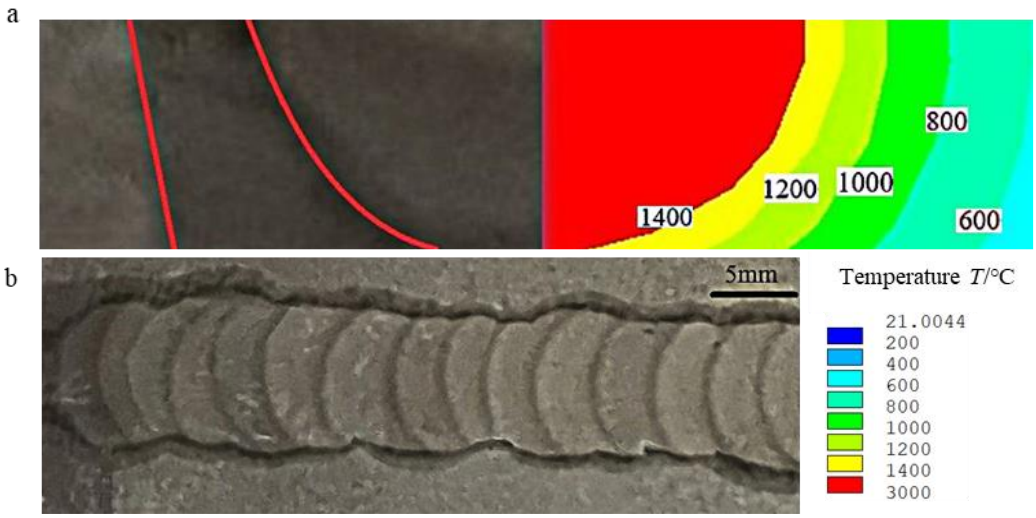

Fig. 9 - (a) Comparison of experimental results and simulated calculation results of weld morphology; (b) weld appearance

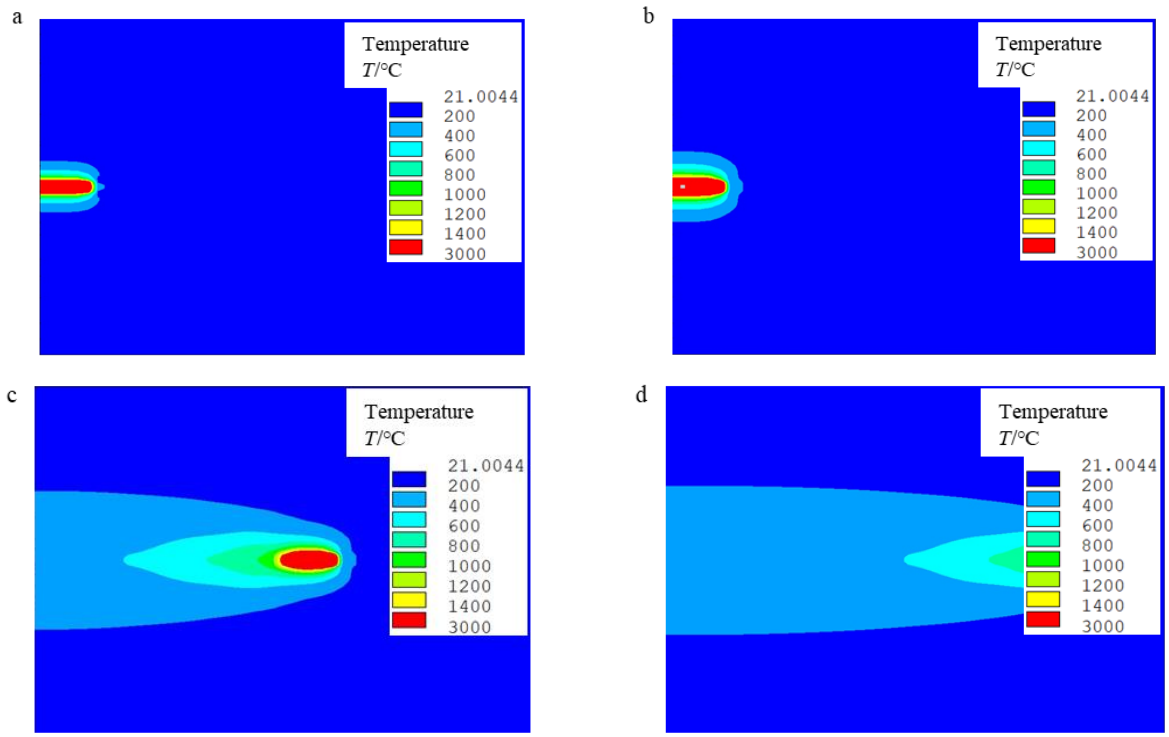

Fig. 10 - Cloud diagram of dynamic evolution of temperature field: (a) 1s; (b) 2s; (c) 12s; (d) 18s

4.3 The Influence of Welding Current On Temperature Field and Molten Pool

There are many factors that affect the welding temperature field. Among them, the size of the process parameters directly determines the size of the heat generation rate. As a result, the effect of process parameters on the welding temperature field is most noticeable. The influence of different currents on the welding temperature field is investigated while the remaining welding parameters stay constant. Weld beads with currents of 185A, 190A, and 195A were taken for analysis.

1). The distribution of the temperature field cloud map when the welding time t=10s. As shown in Fig. 11, the high-temperature range increases with increasing current as the size of the heat source increases. The temperature ranges of 400 °C-600 °C and 800 °C-1000 °C expanded significantly.

2). Temperature-time curve. At the aspect of the welding process, when determining other welding parameters, the fill height of the weld bead increases as the welding current increases, as does the height of weld pool on the side wall and the width of weld pool on the bottom. With the remaining welding parameters unchanged, the currents of different weld beads are altered, and the currents are 185A, 190A, and 195A, respectively. As the size of the heat source increases, the peak temperature also increases. When the current is 185A, the maximum temperature is 1899℃. When the current is 190A, the maximum temperature is 1928℃. When the welding current is 195A, the maximum temperature is 1957 ℃. The maximum temperature increases with the increase of the current. As shown in Fig. 12, the temperature rises extremely rapidly in the area where the welding heat source acts, and the temperature drops rapidly after the leave of heat source.

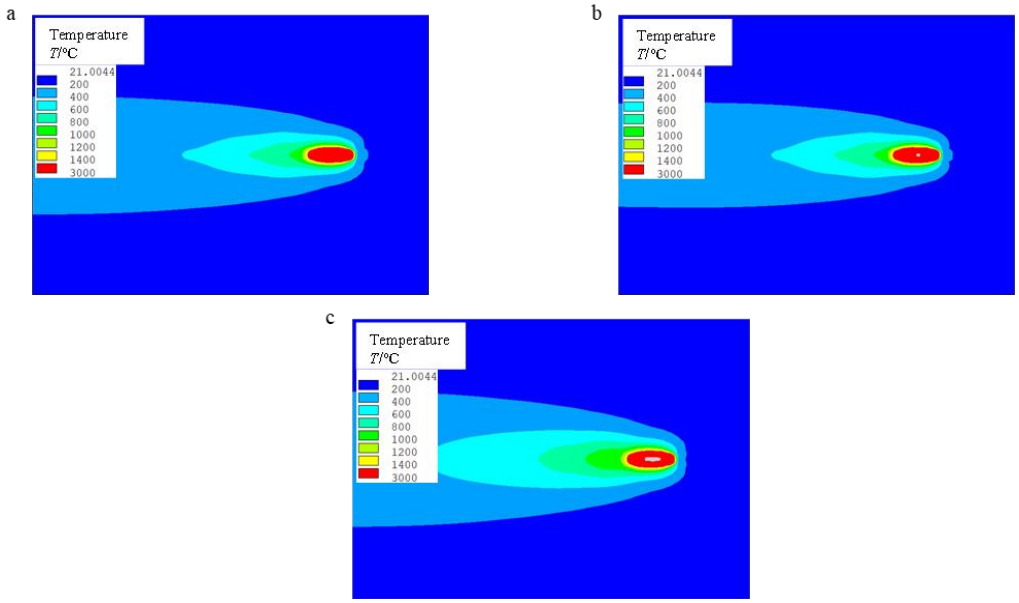

Fig. 11 - Temperature cloud diagram under different currents: (a) I=185A; (b) I=190A; (c) I=195A

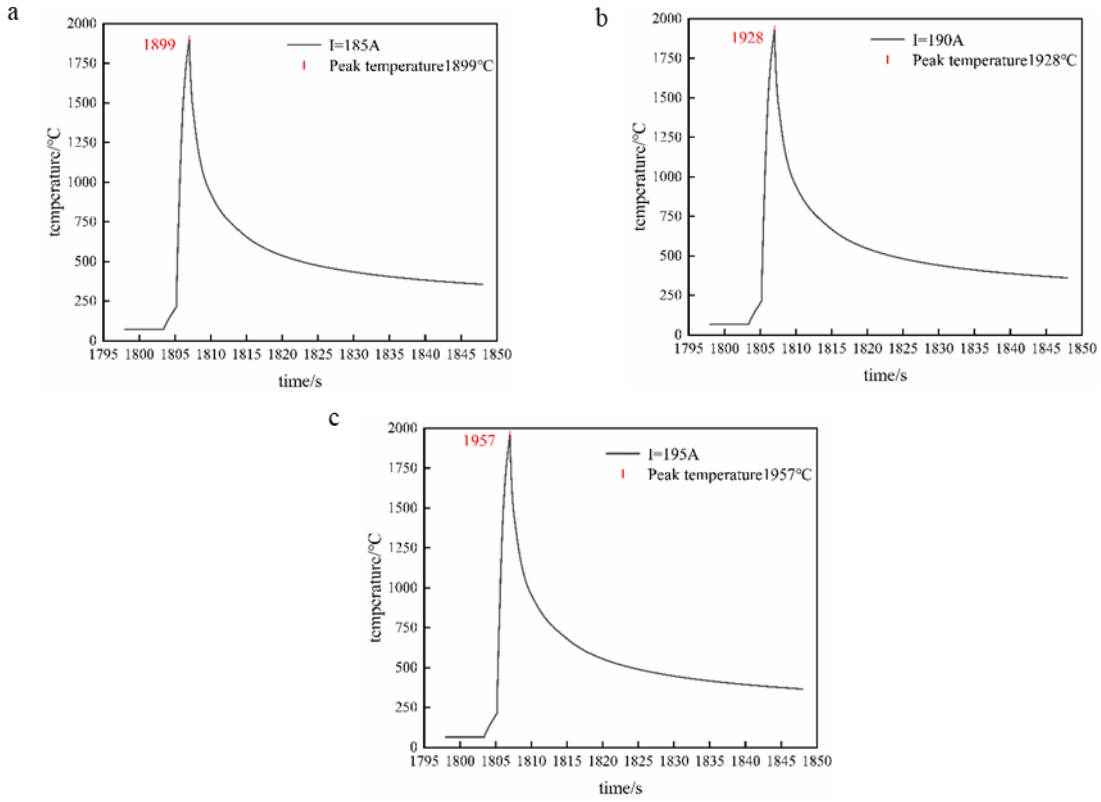

Fig. 12 - Temperature-time curve: (a) I=185A; (b) I=190A; (c) I=195A

Fig. 13 shows a cross-sectional cloud diagram of the molten pool of the welding temperature field under different welding currents. When the welding current is increased from 185A to 195A, the high-temperature area expands significantly. As shown in Fig. 13, the temperature range of 800℃~1000℃ changes most obviously. In Fig. 13, the area within the black wireframe is the weld area, with a length of 4.5mm and a height of 3mm. When the current is 185A, the weld pool area is just larger than the weld area, and incomplete fusion does not occur at the root of the sidewall. When the current is 195A, the molten pool area is further expanded to ensure the good fusion of the sidewalls and roots.

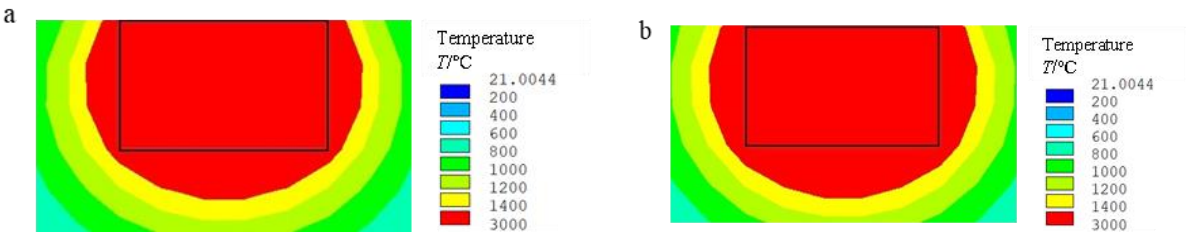

Fig. 13 - The cross-sectional shape of the molten pool under different welding currents:(a)185A; (B)195A

5. Conclusion

This article focuses on the welding problem of the steam turbine valve body of Sharing Cast Steel Co., Ltd. The material of the valve body is ZG13Cr9Mo2Co1NiVNbNB. At present, the main welding method used is manual arc welding, which has low welding efficiency and many consumables. It is prone to defects such as slag inclusion, pores, undercuts, and cracks. In order to address the aforementioned issues, this study first assessed the welding thermal cycle curve through experiments and obtained the macroscopic morphology of the weld. ANSYS finite element software is then used to create a finite element model and simulate the temperature field. The simulation result is compared with the experimentally measured thermal cycle curve. Furthermore, the simulated molten pool morphology is compared to the actual weld macro morphology to validate the model. On this basis, the effect of current on the welding temperature field and the size of the molten pool is investigated further. The following conclusions can be drawn from the preceding research:

(1) When the simulation results are compared to the actual measurement findings, the results show that the simulated thermal cycle curve is near to the welding thermal cycle curve of the welding measurement, and the morphology of the simulated molten pool is basically consistent with the macroscopic morphology of the weld. The feasibility of using a uniform body heat source to simulate the temperature field of ultra-narrow gap welding with flux strips constraining the arc, as well as the reliability of the welding temperature field finite element model, is proved

(2) It is investigated how welding current affects the welding temperature field and the size of the simulated molten pool. The results show that as the welding current increases, so does the peak temperature of the welding temperature field, and the weld width of the simulated molten pool. Incomplete fusion does not occur at the root of the sidewall when the welding current is 185A.

Acknowledgement

It is acknowledged that this research work was supported by the Key Research and Development Plan of the Ningxia Hui Autonomous Region, Ningxia, China (No.2019BDE03005; No. 2019BEB04045；No. 2021BEE03001) and the Malaysia Ministry of Education, University Malaysia Pahang (PGRS1903160).

References

[1] Bolun, D., Xiaoyu, Ni Zhida, et al. (2019). Numerical simulation of arc characteristics in narrow gap TIG welding. International Journal of Mechanical Sciences, 161-162: 105031.

[2] Zhanglan, C., Yunfeng, X., Haijun, Q., et al. (2018). Stress intensity factor-based prediction of solidification crack growth during welding of high strength steel. Journal of Materials Processing Technology, 252, 270-278.

[3] Željko, B., Siegfried, S., & Hinko. W. (2018). The effect of residual stresses on fatigue crack propagation in welded stiffened panels. Engineering Failure Analysis, 84: 346-357.

[4] Liang, Z., Li, P. Y., & Bo, L. Y. (2012). Ultranarrow Gap Welding with Constrained Arc by Flux Strips. Advanced Materials Research, 472-475, 2814-2818.

[5] Turski, M., Francis, J. A., Hurrell, P.R., et al. (2012). Effects of stop-start features on residual stresses in a multipass austenitic stainless steel weld. International Journal of Pressure Vessels and Piping, 89: 9-18.

[6] Dean, D. (2013). Influence of deposition sequence on welding residual stress and deformation in an austenitic stainless steel J-groove welded joint. Materials & Design, 49, 1022-1033.
[7] Yaghi A. H., Hyde T. H., Becker A. A., et al. (2005). Residual stress simulation in welded sections of P91 pipes. Journal of Materials Processing Technology, 167, 480-487.
[8] Mu, Q., Guangxu, C., Zaoxiao, Z., et al. (2017). Numerical Simulation of Temperature Field and Residual Stress in Multi-Pass Welds in 2.25Cr-1Mo-0.25V Steel Plate and Comparison with Experimental Measurements//Volume 1B: Codes and Standards. Waikoloa, Hawaii, USA: American Society of Mechanical Engineers.
[9] Brickstad, B., & Josefson, B.L, (1998). A parametric study of residual stresses in multi-pass butt-welded stainless steel pipes. International Journal of Pressure Vessels and Piping, 75, 11-25.